ACS APPLIED MATERIALS & INTERFACES

Research Article

www.acsami.org

Preparation of Silicon@Silicon Oxide Core–Shell Nanowires from a Silica Precursor toward a High Energy Density Li-Ion Battery Anode

Chuanjian Zhang,[†,∥] Lin Gu,[‡,∥] Nitin Kaskhedikar,[§] Guanglei Cui,*[,†,§] and Joachim Maier*[,§]

[†]Qingdao Institute of Bioenergy and Bioprocess Technology, Chinese Academy of Sciences, No. 189 Songling Road, Laoshan District, Qingdao 266101, P. R. China

[‡]Beijing National Laboratory for Condensed Matter Physics, Institute of Physics, Chinese Academy of Sciences, No. 8, 3rd South Street, Zhongguancun, Haidian District, Beijing 100190, P.R. China

[§]Max Planck Institute for Solid State Research, Heisenbergstasse 1, Stuttgart 70569, Germany

Supporting Information

ABSTRACT: Bulk-quantity silicon@silicon oxide nanowires have been successfully synthesized via a facile high-temperature approach using environment-friendly silica mixed with titanium powders. It is confirmed that the obtained nanowires process a crystalline core and amorphous oxide sheath. The obtained nanowires grow along the [111] direction which catalyzed by spherical silicon@siilcon oxide nanoparticles. The unique one-dimensional structure and thin oxide sheath result in the favorable electrochemical performances, which may be beneficial to the high energy density silicon anode for lithium ion batteries.

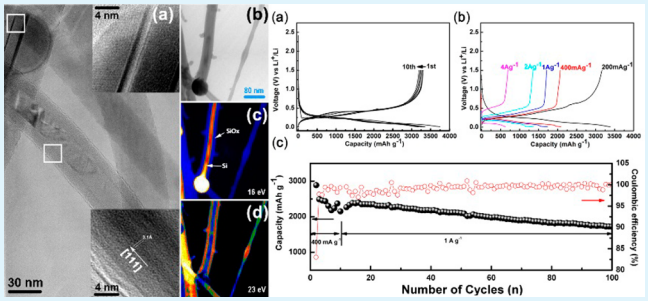

KEYWORDS: *core–shell, batteries, silicon, nanowires, electrochemistry, anode materials*

INTRODUCTION

Nanostructured silicon-based material, especially one-dimensional nanowire, is regarded to be one of the most promising candidates as an anode material for lithium batteries owing to a higher theoretical capacity (4200 mAh g^{-1}) of silicon than that of graphite (372 mAh g^{-1}).[1−3] Moreover, silicon nanowires have attracted great attention in electronics, because it may open new opportunities in the field of silicon nano-electronics,[4] nano-photonics,[5] and nano-biosensors.[6,7] Therefore, the exploration of nanostructured silicon nanowires is one of the most important subjects in the nanostructured material field. Many efforts have been done to prepare silicon nanowires, such as chemical etching,[8] thermal evaporation deposition,[9] chemical vapor deposition (CVD),[10] and supercritical fluid–liquid–solid (SFLS) synthesis.[11] The most popular growth mechanism for silicon nanowires is the vapor–liquid–solid (VLS) mechanism using Au as a catalyst material pioneered by Wagner and Ellis in 1964[12] and advanced by Givarizov.[13] The possibility of fabricating silicon nanowires with other metals except Au has been demonstrated, too.[14] In this VLS process, the metal catalyst is often embedded in the liquid phase to form a droplet during the catalytic growth of the nanowires. At the same time, Si is located at the tip of the wire and moves along with the growing end of the wire. Therefore, this method provides an efficient route to obtain uniform-sized nanowires. In addition, an oxide-assisted-growth method has also been developed to produce large quantities of silicon nanowires.[15] However, toxic silane or expensive catalysts (silicon powder) and complicated instruments are applied among these methods, which limit the potential for large scale applications, especially for anode material of lithium batteries. It is worth noting that silicon materials with an oxide shell may exhibit improved cycling performance due to the formation of a stable SEI layer as well as the compressive stress which limit the extent of lithiation.[16,17] Hence, it is still a great challenge to prepare silicon nanowires with an oxide sheath using a cheap catalyst and environment-benign Si precursor, for example, silica.

Herein, we presented a bulk-quantity silicon@silicon oxide core–shell nanowire preparation method using a facile approach through thermal evaporation of silica mixed with titanium powder. In our case, titanium only plays a role of reduction reagent in contrast to Au which catalyzes the nanowire growth and is detrimental to device functionality.[15,18] More importantly, it should be noted that the growth of the silicon@silicon oxide core–shell nanowires here is controlled by a new mechanism which is different from the conventional VLS. To identify the chemistry distribution of samples, energy-filtered transmission electron microscopy (EFTEM) was performed to acquire composition maps. The results were achieved by collection of the composition-sensitive inelastic electrons suffered from plasmon losses. It has been confirmed by the EFTEM analysis that the obtained nanowires have a

Received: July 20, 2013
Accepted: November 14, 2013
Published: November 14, 2013

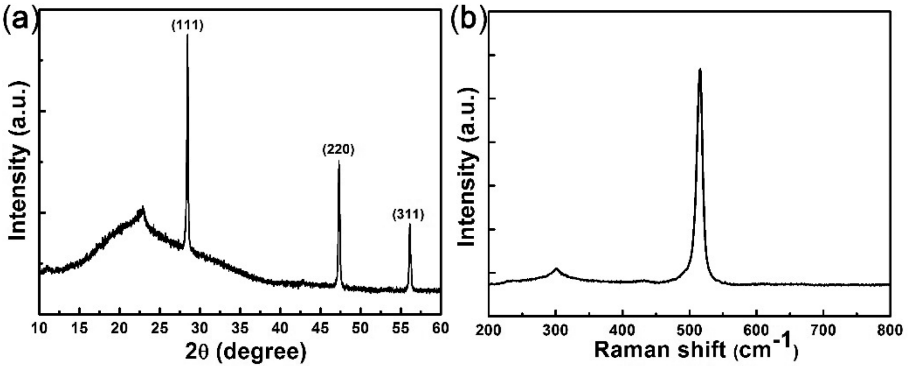

Figure 1. Typical XRD pattern (a) and Raman spectrum (b) of the silicon@silicon oxide core−shell nanowires prepared at a temperature of 1600 °C.

crystalline core surrounded by an amorphous oxide shell. Additionally, superior battery performance would be expected when using silicon@silicon oxide core−shell nanowires as the anode due to the existence of the thin silicon oxide sheath. By combining HRTEM observations with Raman and XRD data, a possible growth mechanism for silicon@silicon oxide core−shell nanowires was presented.

EXPERIMENTAL SECTION

The Preparation of Silicon@Silicon Oxide Core−Shell Nanowires. Firstly, 1 g of silica and 1 g of titanium powder (Sigma-Aldrich, 99.9 %) were mixed and loaded in an alumina boat. Then, the boat with raw materials was placed into a tube furnace and heated up to the desired temperature at a heating speed of 5 °C min^{-1}. Argon (95 %)/hydrogen (5 %) gas was kept feeding into the tube at a flow rate of 60 sccm during the whole reaction. Volatile components were carried by the gas flow, and nanowire began to nucleate and grow on the inner wall of the tube. After the nanowires grew for 6 h, the furnace was shut down and cooled to room temperature. A large amount of sponge-like product with dark yellow color was found deposited on the inner wall of the quartz tube downstream. The deposits were collected from the tube and characterized carefully.

Materials Characterization. X-ray diffraction (XRD) patterns of samples were recorded on a Bruker-AXS Micro-diffractometer (D8 ADVANCE) with Cu Kα radiation (λ = 1.5406 Å) from 10 to 60° at a scanning speed of 4°/min. Resonance Raman spectra were recorded on a JY HR800 Raman spectrophotometer (Horiba Jobin Yvon, France) with 532 nm diode laser excitation. Specimens for transmission electron microscopy (TEM) investigation were prepared by dispersing the silicon@silicon oxide core−shell nanowires on carbon lacey films after dilution in methanol and ultrasonication. High-resolution transmission electron microscopy (HRTEM) was performed using a JEOL 4000EX (JEOL Ltd., Tokyo, Japan) transmission electron microscope operated at an acceleration voltage of 400 keV. Energy-dispersive X-ray (EDX) analysis was carried out using a Noran EDX system attached to a Zeiss 912 microscope (Carl Zeiss, Oberkochen, Germany) operated at 120 keV. Chemical mapping was performed using the Zeiss SESAM microscope operated at 200 keV. The microscope is equipped with an electrostatic Ω-type monochromator and the MANDOLINE filter which provide a routinely achievable energy resolution of better than 100 meV.

Electrochemical Measurements. The electrochemical properties were evaluated by using 2032 coin cells with silicon@silicon oxide core−shell nanowires as active materials. The working electrodes were prepared by mixing silicon@silicon oxide core−shell nanowires, super P, and poly(acrylic) acid binder in a weight ratio of 80:10:10 and pasted on a copper foil followed with drying in a vacuum oven at 120 °C for 8 h. Lithium foil was used as a counter electrode and separated with the working electrodes by a Celgard 2500 polymeric separator. The electrolyte was 1.0 mol L^{-1} $LiPF_6$ in a mixture of ethylene carbonate (EC), dimethyl carbonate (DMC), and diethyl carbonate (DEC) (1:1:1, v/v). Galvanostatic charge−discharge cycling was performed on a LAND battery testing system between 5 mV and 1.5 V vs Li^+/Li. Cyclic voltammetry (CV) measurement was carried out on an IM6 electrochemical workstation between 0 and 1.3 V with a scan rate of 0.1 mV S^{-1}. Electrochemical impedance spectral (EIS) measurements were recorded over the frequency range from 100 kHz to 100 mHz.

RESULTS AND DISCUSSION

X-ray diffraction (XRD) characterization of the product synthesized at 1600 °C is shown in Figure 1a, which demonstrates that the produced nanowires are mixtures of silicon and its oxides. Specifically, the sharp peaks located at 28.4, 47.3, and 56.1° can be completely indexed as the (111), (220), and (311) planes of crystal silicon (JCPDS No. 27-1402), which is consistent with the literature.[1,19,20] Because of the surface oxidization and high surface to volume ratio of nanowires, the broad hump at about 22.5° corresponds to the amorphous silicon oxide in the product.[21] This also could be confirmed by the transmission electron microscopy images in the following discussion. No diffraction peaks of metallic Ti were detected in the XRD pattern. This result may imply that Ti particles play only a reduction reagent role rather than catalyst for nanowire growth.

Further structural information is provided by the Raman spectrum in Figure 1b. The spectrum shows two peaks located at 300 and 516 cm^{-1} corresponding to the second-order transverse acoustic phonon mode (2TA) and the first-order transverse optical phonon mode (TO) of silicon, respectively.[22] Additionally, the peak at 516 cm^{-1} is broad, strongly asymmetric, and a little blue-shifted compared to that of a single silicon crystal previously reported, which may be ascribed to the phonon confinement effect or masking effect.[23] This is the typical characteristic of silicon nanowires covered with some amorphous silicon oxides.[16]

As shown in Figure 2, the morphology and chemistry distribution of silicon@silicon oxide core−shell nanowires grown at 1600 °C were investigated by both HRTEM and EFTEM techniques. It can be seen from the BF image and the HRTEM micrographs acquired on the regions marked by the white box in Figure 2a that both the tip and the wire of the nanowires are well crystalline surrounded by amorphous oxide layers with a thickness of about 10 nm. The clear lattice fringes in the inset of Figure 2a demonstrate that the nanowires are parallel to the [111] direction, which agrees with the results obtained by Wang et al.[24] Generally, nanowires with catalyst nanoparticles embedded in the tip were considered as a typical

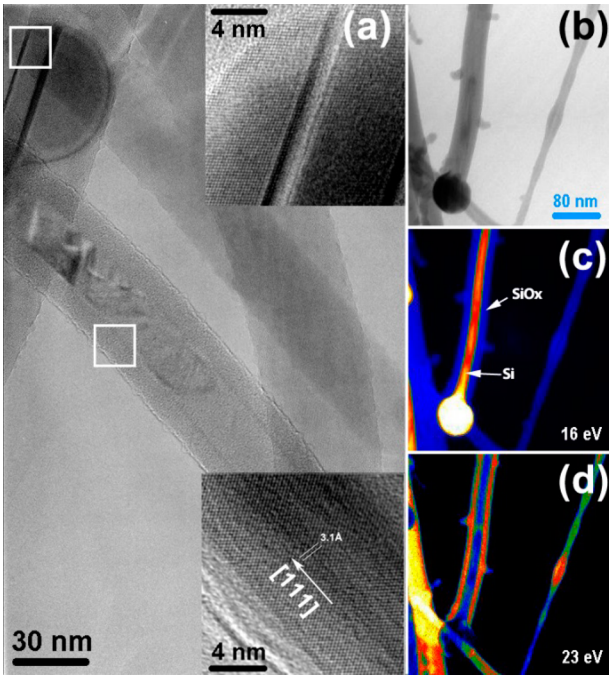

Figure 2. Typical HRTEM and EFTEM images of silicon@silicon oxide core−shell nanowires grown at 1600 °C. (a) HRTEM micrographs acquired on the tip and wire regions marked by the white box are shown at the inset of the bright-field (BF) diffraction contrast image; elemental mappings of silicon and silicon oxide acquired at the corresponding plasmon losses at 16 and 23 eV are shown in parts c and d with the corresponding BF zero-loss filtered elastic images shown in part b. The intensity is illustrated by the color temperature method, and the colors would be changed with the increased energy loss. When the plasmon loss is 16 eV (part c), the yellow core indicated the silicon with high counts and the blue sheath corresponded to silicon oxide with low counts.

feature of conventional metal-catalyzed VLS growth.[18] Obviously, no catalyst metal was observed from the HRTEM of the tip in our case which implied a different growth mechanism compared to the VSL growth. Further composition distributions of the obtained core−shell nanowires are shown in Figure 2c and d, while the corresponding BF zero-loss filtered elastic images are shown in Figure 2b. From the composition maps, it is observed that both the tip and the middle of the wires consist of silicon, while silicon oxide is found mainly from the outside. With the aim to define the growth mechanism of the silicon@silicon oxide core−shell nanowires further, an EFTEM test of the sample obtained at a lower temperature was performed.

At a growth temperature of 1400 °C, most of the silicon materials were found to form spherical particles with oxide surrounding as revealed by a BF zero-loss filtered elastic image shown in Figure 3a. It is interesting to see that the particles with an average size of 25 ± 5 nm, aligned with (111) planes, the directions which were marked with white arrows in the HRTEM of a single silicon@silicon oxide nanoparticle (inset of Figure 3). These observations agreed with the results given in Figure 2 that [111] is the preferred growth direction for silicon nanowire growth. Parts b and d of Figure 3 reveal the silicon and silicon oxide mapping acquired at the corresponding plasmon losses at 8 and 23 eV, respectively, which are false colored using the color temperature method. Note that the SiO_x plasmon has similar energy to carbon $\sigma + \pi$ plasmon; this

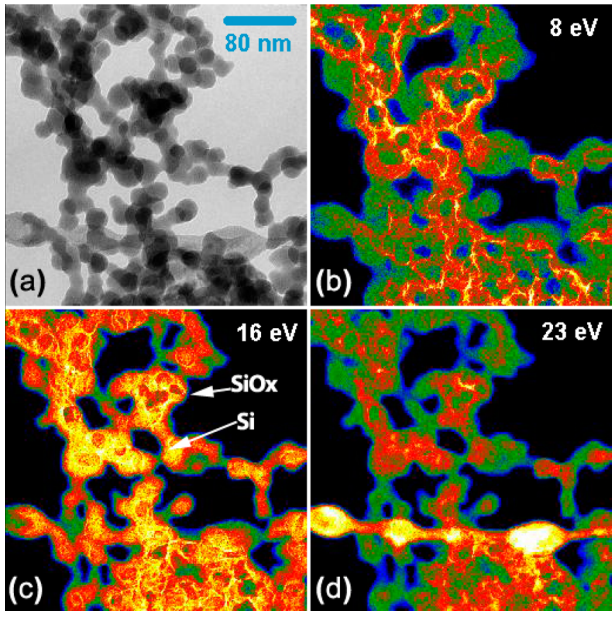

Figure 3. Typical EFTEM images of the silicon@silicon oxide nanoparticles grown at 1400 °C. (a) BF zero-loss filtered micrograph using elastic electrons and its (b, d) elemental mapping acquired at the corresponding plasmon losses at 8, 16, and 23 eV, respectively. The inset is the HRTEM image of an individual silicon@silicon oxide nanoparticle. The blue shell corresponding to silicon oxide could be seen clearly.

explains the inclusion of carbon signal at 23 eV shown in Figure 3d. To support our observation, the interface plasmon between the silicon core and its oxide sheath was acquired at the energy loss of 16 eV shown in Figure 3c. This map confirms the above chemical distribution analysis manifesting the surrounding of oxide shells around the silicon nanospheres.

By combining all the results listed above, a possible mechanism which is different from the conventional VSL mechanism for silicon nanowire growth is presented in Figure 4. Due to the lower negative heat of silicon oxide than titanium

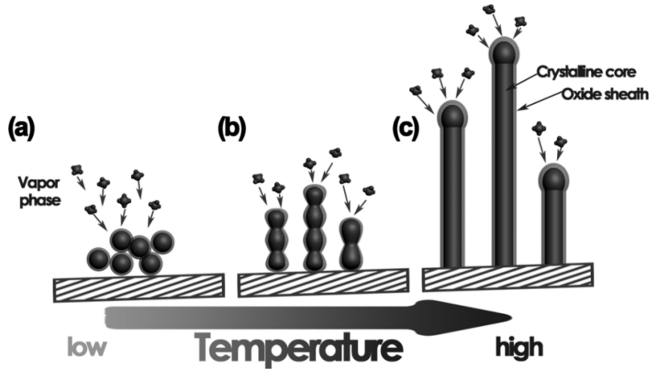

Figure 4. Schematic diagram of silicon@silicon oxide core−shell nanowire growth.

oxide, titanium can reduce the silica raw powder to Si or SiO_x ($x \geq 1$) thermodynamically.[25] Moreover, titanium powders didn't participate in the following growth process of silicon nanowires which had been confirmed by the XRD results in Figure 1a and EFTEM images in Figure 2.

We believe that spherical silicon nanoparticles with an oxide shell act as a catalyst for continuous nanowire growth. Initially,

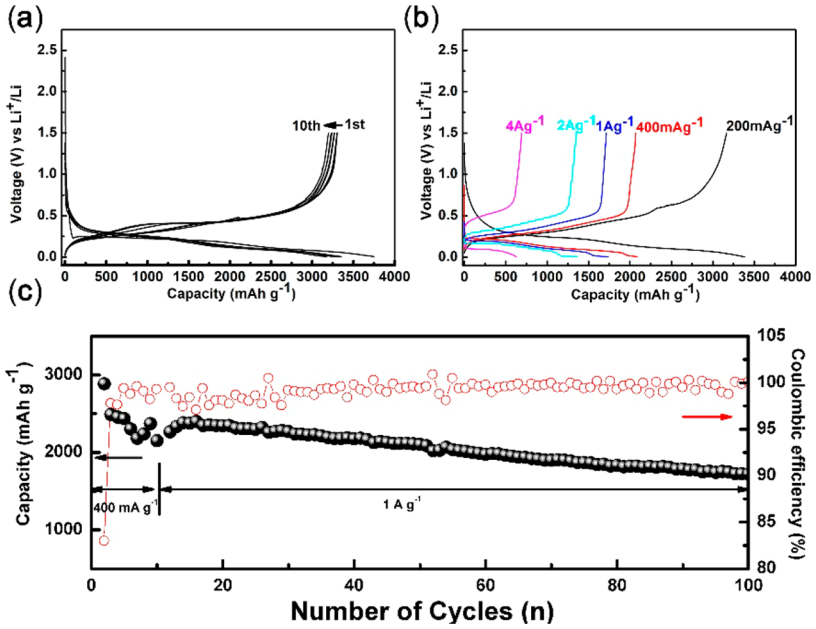

Figure 5. Electrochemical performance of the silicon@silicon oxide core−shell nanowires: (a) galvanostatic discharge−charge curves for the first 10 cycles at a current density of 200 mA g^{-1}; (b) rate capability and (c) cycling performance of the silicon@silicon oxide core−shell nanowires.

due to the existence of titanium, reduction reaction was carried out in the raw materials. Vapor materials generated from the mixture powders (Figure 4a) mainly contained SiO_x ($x \geq 1$) and Si. Nucleation occurred when the vapor materials deposited on the inner wall of the tube. Meanwhile, it is reported that the metastable volatile SiO component could be easily decomposed to Si and SiO_2.[26,27] Because of the lowest surface energy of the Si(111) plane, recrystallization of silicon inside the nucleus was subsequently proceeded. As a result, spherical nanoparticles with a crystalline core which oriented growth along the [111] direction were observed in the inset of Figure 3. However, when the reaction temperature of the raw mixture was increased further (1600 °C), more volatile materials deposited on the spherical silicon@silicon oxide nanoparticles and formed a strong Si−Si bond along the [111] direction (Figure 4c).[28] The mass transportation rate to the tips of the nuclei should be much higher than to their edge side.[27] At the same time, oxygen atoms might be expelled by the silicon atoms and diffuse to the edge, forming a chemically inert silicon oxide which retards the sideways growth of the nanowire. Finally, nanowires along the [111] direction with a crystalline core and amorphous sheath were synthesized.

The electrochemical performances of the silicon@silicon oxide core−shell nanowires were evaluated by assembling a half test cell. Figure 5a displays the first 10 discharge−charge profiles of the silicon@silicon oxide core−shell nanowires cycled at a current density of 200 mA g^{-1} between the voltage limits of 5 mV to 1.5 V. It can be seen that there is a very long and flat voltage plateau around 0.25 V. This may be ascribed to the formation of Li_xSi alloy according to the previous literature.[2,29−32] CV curves in Figure S1 (Supporting Information) show good agreement with the voltage profile and the data reported before.[33] The anodic peak that appeared at 0.56 V could be ascribed to dealloying of Li_xSi alloys. The discharge and charge capacity of the first cycle were 3757 and 3312 mAh g^{-1}, respectively, corresponding to a Coulombic efficiency of 88%. It is well known that the irreversible capacities loss was mainly caused by the formation of a solid electrolyte interface (SEI) formed by the side reaction between active material and the electrolyte.[33−37] For Si and Ge materials, due to the remarkable volume expansion and contraction during lithium insertion and extraction, the active particles were pulverized and accompanied a large amount of new formation surface electrolyte. Undoubtedly, electrolyte and lithium salts would continuously consume and lead to a low Coulombic efficiency.[1,19,38−40] Note that the thickness of the thin oxide layer may have a remarkable influence on the electrochemical performance of a silicon anode.[41] In our case, the nanoscale silicon oxide may act as a ceramic stabilizer and forms a favorable and stable interface between the crystalline core and electrolyte, as well as maintains the integrity of the electrode.[42] In addition, the weight portion of oxygen measured with an energy dispersive X-ray spectrometer (EDX) (Table S1, Supporting Information) is about 7.64 %. This means that the oxide sheath may lead to a lesser contribution to the irreversible capacity loss. Hence, less consumption of electrolyte and lithium could be achieved and a high Coulombic efficiency could be achieved. More recently, Guo and Cho et al. demonstrated that nano Ge may exhibit a catalytic effect in Ge/Ge dioxide nanocomposite which could realize an enhanced Coulombic efficiency and cyclic stability.[43] In our case, a similar catalytic reaction may also take place on the interface of the crystalline silicon core and oxide sheath. However, detailed reasons for the improved kinetics need to be investigated further. The silicon@silicon oxide core−shell nanowires also exhibit fair rate capability, as shown in Figure 5b. The reversible capacities were 1736, 1360, and 627 mAh g^{-1} when the current densities increased to 1, 2, and 4 A g^{-1}. Another valuable feature of the core−shell nanowires is the cycling performance presented in Figure 5c. As is displayed, after 100 cycles at a current density of 1 A g^{-1}, the reversible capacity of the silicon@silicon oxide core−shell nanowires is still as high as 1640 mAh g^{-1}. The cyclic stability may be also ascribed to the unique core−shell structure. Specifically, the oxide layer can generate compressive stress in the silicon core which could limit the extent of lithium insertion. Consequently,

a highly reversible capacity could be achieved.[17,44,45] In addition, the 1D structure of the nanowires was beneficial to relaxation of the strain generated from the silicon volume expansion.[1] Note that the impedance semicircles after cycling exhibited an increased size compared to the one before cycling in Figure S2 (Supporting Information). This may ascribed to the poor electrical conductivity of samples without any conductive coating.

CONCLUSIONS

In conclusion, bulk-quantity silicon@silicon oxide core−shell nanowires were explored via a high temperature reduction method from a cheap silica precursor. XRD and HRTEM results reveal that it is the spherical silicon nanoparticles with an oxide shell rather than titanium powders that catalyze the nanowires grown along the [111] direction. The as-obtained silicon@silicon oxide core−shell nanowires exhibited a favorable rate and cycling performance which were benefited from the unique core−shell structure. The low cost synthesis routes and the good performances endow these silicon@silicon oxide nanowires a promising anode material for high-power Li-ion batteries.

ASSOCIATED CONTENT

Supporting Information

CV curves, EDX results, and EIS of the silicon@silicon oxide core−shell nanowires. This material is available free of charge via the Internet at http://pubs.acs.org.

AUTHOR INFORMATION

Corresponding Authors

*E-mail: cuigl@qibebt.ac.cn. Fax: (+86) 532-80662744.
*E-mail: s.weiglein@fkf.mpg.de. Fax: (+49)711-6891722.

Author Contributions

‖These authors contributed equally.

Notes

The authors declare no competing financial interest.

ACKNOWLEDGMENTS

This work was supported by The National High Technology Research and Development Program of China (863 Program, No. 2013AA050905), Key Research Program of the Chinese Academy of Sciences (Grant No. KGZD-EW-202-2), National Natural Science Foundation of China (Grant No. 21275151, 21271180), Doctoral Fund of Shandong Province (BS2012NJ011), and the Key Technology Research Projects of Qingdao (No. 12-4-1-24-gx). The authors are indebted to the Max Planck Society and acknowledge support in the framework of the ENERCHEM project.

REFERENCES

(1) Chan, C. K.; Peng, H.; Liu, G.; McIlwrath, K.; Zhang, X. F.; Huggins, R. A.; Cui, Y. *Nat. Nanotechnol.* **2008**, *3*, 31−35.
(2) Cui, L.-F.; Ruffo, R.; Chan, C. K.; Peng, H.-L.; Cui, Y. *Nano Lett.* **2008**, *9*, 491−495.
(3) Wang, B.; Li, X.-L.; Luo, B.; Zhang, X.-F.; Shang, Y.-Y.; Cao, A.-Y.; Zhi, L.-J. *ACS Appl. Mater. Interfaces* **2013**, *5*, 6467−6472.
(4) Weisse, J. M.; Lee, C. H.; Kim, D. R.; Zheng, X. L. *Nano Lett.* **2012**, *12*, 3339−3343.
(5) Bronstrup, G.; Jahr, N.; Leiterer, C.; Csáki, A.; Fritzsche, W.; Christiansen, S. *ACS Nano* **2010**, *4*, 7113−7122.
(6) Hakim, M. M. A.; Lombardini, M.; Sun, K.; Giustiniano, F.; Roach, P. L.; Davies, D. E.; Howarth, P. H.; de Planque, M. R. R.; Morgan, H.; Ashburn, P. *Nano Lett.* **2012**, *12*, 1868−1872.
(7) Kong, T.; Su, R.-G.; Zhang, B.-B.; Zhang, Q.; Cheng, G.-S. *Biosens. Bioelectron.* **2012**, *34*, 267−272.
(8) Huang, Z.-P.; Wang, R.-X.; Jia, D.; Maoying, L.; Humphrey, M. G.; Zhang, C. *ACS Appl. Mater. Interfaces* **2012**, *4*, 1553−1559.
(9) Pan, H.; Lim, S.; Poh, C.; Sun, H.; Wu, X.; Feng, Y.; Lin, J. *Nanotechnology* **2005**, *16*, 417.
(10) Hu, L.; Wu, H.; Hong, S. S.; Cui, L.; McDonough, J. R.; Bohy, S.; Cui, Y. *Chem. Commun.* **2011**, *47*, 367−369.
(11) Chockla, A. M.; Harris, J. T.; Akhavan, V. A.; Bogart, T. D.; Holmberg, V. C.; Steinhagen, C.; Mullins, C. B.; Stevenson, K. J.; Korgel, B. A. *J. Am. Chem. Soc.* **2011**, *133*, 20914−20921.
(12) Wagner, R. S.; Ellis, W. C. *Appl. Phys. Lett.* **1964**, *4*, 89−90.
(13) Givargizov, E. I. *J. Cryst. Growth* **1975**, *31*, 20−30.
(14) Ahmad, I.; Fay, M.; Xia, Y.-D.; Hou, X.-H.; Kennedy, A.; Zhu, Y.-Q. *J. Phys. Chem. C* **2009**, *113*, 1286−1292.
(15) Wang, N.; Tang, Y. H.; Zhang, Y. F.; Lee, C. S.; Bello, I.; Lee, S. T. *Chem. Phys. Lett.* **1999**, *299*, 237−242.
(16) Hu, Y.-S.; Demir-Cakan, R.; Titirici, M.-M.; Müller, J.-O.; Schlögl, R.; Antonietti, M.; Maier, J. *Angew. Chem. Int. Ed.* **2008**, *47*, 1645−1649.
(17) McDowell, M. T.; Lee, S. W.; Ryu, I.; Wu, H.; Nix, W. D.; Choi, J. W.; Cui, Y. *Nano Lett.* **2011**, *11*, 4018−4025.
(18) Lensch-Falk, J. L.; Hemesath, E. R.; Perea, D. E.; Lauhon, L. J. *J. Mater. Chem.* **2009**, *19*, 849−857.
(19) Magasinski, A.; Dixon, P.; Hertzberg, B.; Kvit, A.; Ayala, J.; Yushin, G. *Nat. Mater.* **2010**, *9*, 353−358.
(20) Yu, D. P.; Bai, Z. G.; Ding, Y.; Hang, Q. L.; Zhang, H. Z.; Wang, J. J.; Zou, Y. H.; Qian, W.; Xiong, G. C.; Zhou, H. T.; Feng, S. Q. *Appl. Phys. Lett.* **1998**, *72*, 3458−3460.
(21) Zhang, Y. F.; Tang, Y. H.; Wang, N.; Yu, D. P.; Lee, C. S.; Bello, I.; Lee, S. T. *Appl. Phys. Lett.* **1998**, *72*, 1835−1837.
(22) Chen, X. H.; Xing, Y. J.; Xu, J.; Xiang, J.; Yu, D. P. *Chem. Phys. Lett.* **2003**, *374*, 626−630.
(23) Meier, C.; Lüttjohann, S.; Kravets, V. G.; Nienhaus, H.; Lorke, A.; Wiggers, H. *Phys. E (Amsterdam, Neth.)* **2006**, *32*, 155−158.
(24) Gole, J. L.; Stout, J. D.; Rauch, W. L.; Wang, Z. L. *Appl. Phys. Lett.* **2000**, *76*, 2346−2348.
(25) Kubaschewski, O.; Alcock, C. B. *Metallurgical Thermochemistry*, 5th ed.; Pergamon Press: New York, 1979.
(26) Setiowati, U.; Kimura, S. *J. Am. Ceram. Soc.* **1997**, *80*, 757−760.
(27) Zhang, Y. F.; Tang, Y. H.; Wang, N.; Lee, C. S.; Bello, I.; Lee, S. T. *J. Cryst. Growth* **1999**, *197*, 136−140.
(28) Zhang, R. Q.; Lifshitz, Y.; Lee, S. T. *Adv. Mater.* **2003**, *15*, 635−640.
(29) Zhou, X.-S.; Yin, Y.-X.; Wan, L.-J.; Guo, Y.-G. *Chem. Commun.* **2012**, *48*, 2198−2200.
(30) Yin, Y.-X.; Xin, S.; Wan, L.-J.; Li, C.-J.; Guo, Y.-G. *J. Phys. Chem. C* **2011**, *115*, 14148−14154.
(31) Ng, S.-H.; Wang, J.-Z.; Wexler, D.; Konstantinov, K.; Guo, Z.-P.; Liu, H.-K. *Angew. Chem., Int. Ed.* **2006**, *45*, 6896−6899.
(32) Chou, S.-L.; Zhao, Y.; Wang, J.-Z.; Chen, Z.-X.; Liu, H.-K.; Dou, S.-X. *J. Phys. Chem. C* **2010**, *114*, 15862−15867.
(33) Zhou, X.-S.; Yin, Y.-X.; Cao, A.-M.; Wan, L.-J.; Guo, Y.-G. *ACS Appl. Mater. Interfaces* **2012**, *4*, 2824−2828.
(34) Park, C.-M.; Kim, J.-H.; Kim, H.; Sohn, H.-J. *Chem. Soc. Rev.* **2010**, *39*, 3115−3141.
(35) He, Y.; Yu, X.-Q.; Wang, Y.-H.; Li, H.; Huang, X.-J. *Adv. Mater.* **2011**, *23*, 4938−4941.
(36) Xue, L.-G.; Xu, G.-J.; Li, Y.; Li, S.-L.; Fu, K.; Shi, Q.; Zhang, X.-W. *ACS Appl. Mater. Interfaces* **2012**, *5*, 21−25.
(37) Chockla, A. M.; Panthani, M. G.; Holmberg, V. C.; Hessel, C. M.; Reid, D. K.; Bogart, T. D.; Harris, J. T.; Mullins, C. B.; Korgel, B. A. *J. Phys. Chem. C* **2012**, *116*, 11917−11923.
(38) Wang, L.; He, X.-M.; Li, J.-J.; Sun, W.-T.; Gao, J.; Guo, J.-W.; Jiang, C.-Y. *Angew. Chem., Int. Ed.* **2012**, *51*, 9034−9037.

(39) Zhou, M.; Cai, T.-W.; Pu, F.; Chen, H.; Wang, Z.; Zhang, H.-Y.; Guan, S.-Y. *ACS Appl. Mater. Interfaces* **2013**, *5*, 3449−3455.
(40) Seng, K. H.; Park, M.-H.; Guo, Z. P.; Liu, H. K.; Cho, J. *Angew. Chem. Int. Ed.* **2012**, *51*, 5657−5661.
(41) Sim, S.; Oh, P.; Park, S.; Cho, J. *Adv. Mater.* **2013**, *25*, 4498−4503.
(42) Jamnik, J.; Dominko, R.; Erjavec, B.; Remskar, M.; Pintar, A.; Gaberscek, M. *Adv. Mater.* **2009**, *21*, 2715−2719.
(43) Seng, K. H.; Park, M.-h.; Guo, Z.-P.; Liu, H.-K.; Cho, J. *Nano Lett.* **2013**, *13*, 1230−1236.
(44) Son, S.-B.; Kim, S. C.; Kang, C. S.; Yersak, T. A.; Kim, Y.-C.; Lee, C.-G.; Moon, S.-H.; Cho, J. S.; Moon, J.-T.; Oh, K. H.; Lee, S.-H. *Adv. Energy Mater* **2012**, *2*, 1226−1231.
(45) Einhorn, M.; Conte, F. V.; Kral, C.; Fleig, J. *IEEE Trans. Appl. Ind.* **2012**, *48*, 736−741.